Raman-scattering studies of silicon-implanted gallium arsenide: The role of amorphicity

M. Holtz, R. Zallen, Art E. Geissberger, and R. A. Sadler

Citation: Journal of Applied Physics **59**, 1946 (1986); doi: 10.1063/1.336423
View online: http://dx.doi.org/10.1063/1.336423
View Table of Contents: http://scitation.aip.org/content/aip/journal/jap/59/6?ver=pdfcov
Published by the AIP Publishing

Raman-scattering studies of silicon-implanted gallium arsenide: The role of amorphicity

M. Holtz and R. Zallen
Department of Physics, Virginia Tech, Blacksburg, Virginia 24061

Art E. Geissberger and R. A. Sadler
ITT Gallium Arsenide Technology Center, Roanoke, Virginia 24019

(Received 28 October 1985; accepted for publication 3 December 1985)

A series of Raman-scattering experiments were carried out on GaAs implanted with Si^+ and with SiF_3^+ ions, both before and after annealing, for samples subjected to fluences spanning a wide range. The implantation-induced amorphization of the damage layer was cleanly observed via the evolution, with increasing fluence, of the broad three-band continuum of amorphous GaAs which extends from near zero up to 300 cm^{-1}. Annealing recovers the simple line spectrum of crystalline GaAs, but with a changed longitudinal-optical/transverse-optical intensity ratio which indicates a departure from epitaxial regrowth. Three lines observed near 400 cm^{-1} in heavily implanted samples were identified with silicon vibrational local modes. The effect of annealing on these local-mode lines is *not* an intensity increase but is instead a line *narrowing* which reveals an annealing-induced sharpening of the distribution of local settings sampled by the substitutional silicons. In particular, a line (at 381 cm^{-1}) assigned to the Si-at-a-Ga-site donor impurity is clearly seen *before* annealing, even though annealing is needed to transform the highly resistive implanted material into semiconducting *n*-type GaAs. We propose that the primary role of annealing in the "electrical activation" of implanted semiconductors is *not* to shift the impurity atoms into substitutional donor or acceptor sites (they already occupy such sites), but is instead to recover the high carrier mobility of the crystalline form. "Healing" and "activation" thus correspond to the *same* process, the elimination of amorphicity.

I. INTRODUCTION

With the increasing technological importance of ion implantation as a method for introducing dopants into semiconductor device structures, interest has grown in attempting to understand (and thereby control) the implantation-induced structural disorder produced within the "damage layer," as well as the subsequent annealing-induced "healing" of the damage and electrical "activation" of the dopant. Conversely, the possibility of using implantation to "tune" the degree of disorder in a controlled way has provided a new scientific tool for studying such phenomena as the amorphization process.[1–3] A powerful technique for probing the atomic-scale structure of the implanted layer is the use of Raman-scattering experiments in which the optical penetration depth of the incident laser beam is chosen to be less than, or comparable to, the ion penetration depth.[2–4]

In this paper, we report the results of a systematic Raman-scattering investigation of GaAs samples which have been implanted with Si^+ or SiF_3^+ ions. Structural effects on the host semiconductor of implantations of varying ion fluence and of annealing are described, and annealing-induced changes in Raman bands associated with local vibrational modes of substitutionally incorporated silicon are also reported and correlated with electrical activation. Among our findings: "healing" and "activation" are not separate processes, both correspond to the elimination of amorphicity.

II. EXPERIMENT

The starting single-crystal material was undoped semi-insulating GaAs grown by the liquid-encapsulated Czochralski method. Wafers with (100) orientation were polished and etched with 5:1:1 H_2SO_4:H_2O_2:H_2O, yielding optical quality flat surfaces. Ultraviolet reflectivity spectra, a sensitive test of surface quality and crystallinity, clearly revealed the characteristic interband peaks of crystalline GaAs. Implantation was carried out with the ion beam at 7° from the (100) normal, using either $^{28}Si^+$ or SiF_3^+ ions at 120 keV. Fluence ranged from 6×10^{12} to 1×10^{16} cm^{-2}. The implant stage was not cooled, so that substrate temperatures varied somewhat with both flux and fluence.

For the annealing studies, implanted samples were encapsulated with 2000 Å of chemical-vapor-deposited SiO_2 to prevent arsenic loss. After annealing and prior to Raman measurements, this film was removed by hydrofluoric acid. The anneal was either a standard furnace anneal (SFA) at 850 °C for 20 min in flowing nitrogen with 10% hydrogen, or a rapid thermal anneal (RTA) in a commercial quartz-halogen-lamp system at about 940 °C for 12 s in pure nitrogen. Electrical sheet resistances of the samples were measured with a noncontacting eddy current instrument, and depth profiles of carrier concentration were estimated by electrochemical capacitance-voltage (*C-V*) measurements. All annealed samples were shown to be *n*-type GaAs by Hall measurements.

Raman-scattering measurements were taken at room temperature, using a SPEX 1403 double monochromator equipped with holographic gratings and internal spatial filtering (via a fourth slit). The detector was a cooled GaAs-photocathode photomultiplier, and photon-counting electronics was employed. Repetitive scans were taken under computer control; data accumulation times varied from 0.5

 0021-8979/86/061946-06$02.40

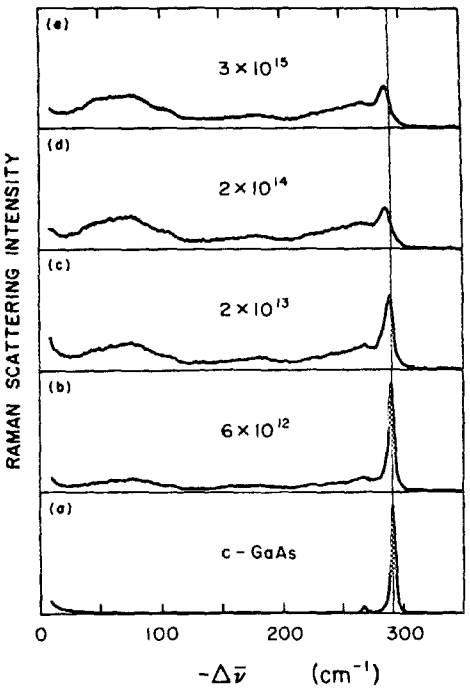

FIG. 1. The effect of ion fluence on the host-lattice Raman spectrum of silicon-implanted GaAs. Each curve is labeled by the $^{28}Si^+$ ion fluence in units of ion/cm^2, except for the lowest curve which is for the pristine crystal wafer. For this figure and the succeeding ones, the spectral slit width employed was 2.5 cm^{-1}, appreciably less than the width of any of the features observed. These are room-temperature spectra, obtained in back reflection using 5145-Å excitation.

to 40 h. The green line (5145 Å, 2.41 eV) of an argon ion laser was the principal form of excitation. A quasi-backscattering ("reflection Raman") geometry was used, with the laser beam incident at 40° from the normal (less than 9° from the normal *inside* the sample) and the scattered radiation was collected in a cone centered around the normal. Laser power was kept below 50 mW at the sample.

At a photon energy of 2.41 eV, the optical penetration depth in crystalline GaAs (c-GaAs) is 1100 Å.[5] In amorphous GaAs (a-GaAs), it is about 300 Å.[6] Both of these values are less than the reported value of the damage-layer thickness, which is roughly 2000 Å.[7] Our own C-V measurements also find an ion penetration depth of about 2000 Å. Thus, the use of the argon green line in these Raman experiments effectively probes the shallow ion-implanted region.

III. AMORPHIZATION AND RECOVERY OF THE GaAs LATTICE

Figure 1 displays a sequence of Raman-scattering results for 120-keV $^{28}Si^+$ implantations with fluences ranging up to 3×10^{15} cm^{-2}. Raman-scattering intensity is plotted against the frequency downshift $-\Delta\bar{\nu}$. Here $\Delta\bar{\nu}=\bar{\nu}-\bar{\nu}_L$, where $\bar{\nu}_L$ is the frequency of the laser line and $\bar{\nu}$ is the frequency of the scattered light. Frequency is given in terms of the wave number equivalent ($\bar{\nu}=1/\lambda=\nu/c=E/hc$, where λ is wavelength, ν is frequency, and E is photon energy). The clean spectrum of the unimplanted crystal (c-GaAs) is dominated by the sharp $q=0$ longitudinal-optical (LO) phonon line at 292 cm^{-1}. Also observed, very weakly, is the $q=0$ transverse-optical (TO) line at 268 cm^{-1}. For backscattering geometry along the (100) direction in c-GaAs, the TO line is symmetry forbidden.[8] Its appearance in the c-GaAs spectrum in Fig. 1 could be due to our small experimental deviation from backscattering, but in fact this line evidently appears even in a strict backscattering geometry.[3]

The evolution of the spectra of Fig. 1, with increasing implantation dose, exhibits the development of a broad three-band continuum which extends from $\bar{\nu}=0$ to $\bar{\nu}=300$ cm^{-1}. We interpret this as the Raman signature of amorphous GaAs. It resembles results reported earlier on sputtered a-GaAs,[9] although the comparison to a-GaAs prepared by conventional (i.e., vapor phase) methods is difficult to make because our spectra are much better defined than the available data on sputtered a-GaAs, especially at low frequencies. Also, our spectra are significantly cleaner and more complete (observed down to 15 cm^{-1} before ap-

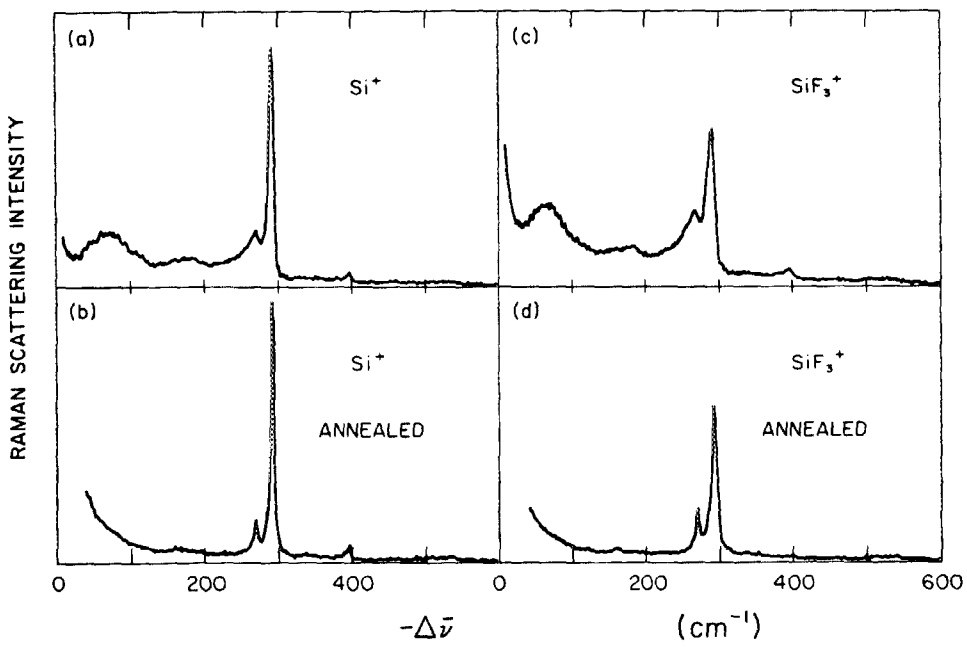

FIG. 2. The effect of annealing on the Raman spectra of Si-implanted and SiF_3-implanted GaAs. Implantation was for an ion fluence of 10^{16} cm^{-2} and an ion energy of 120 keV; annealing was a rapid thermal anneal (950 °C; 12 s). These spectra, as well as the others presented in this paper, were obtained with the incident beam polarized in the scattering plane and with both polarizations collected for the scattered beam.

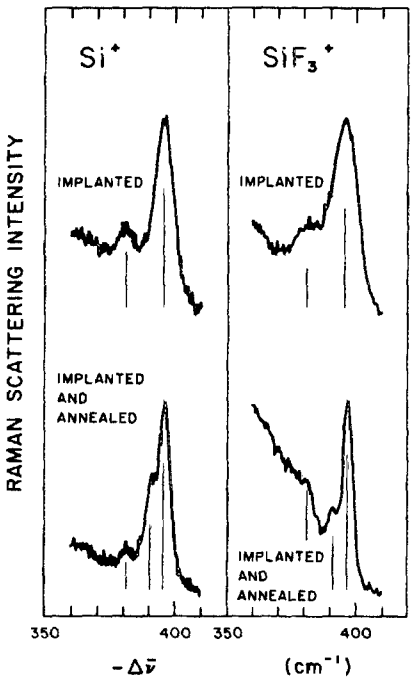

FIG. 3. Detailed scans of the local-mode region of the samples of Fig. 2.

preciable competition appears from parasitic scattering) than earlier data[2,10] on silicon-implanted GaAs.

The simplest way to understand the overall features of the *a*-GaAs spectrum is via disorder-induced selection-rule breakdown. While *only* the $q = 0$ LO mode is Raman active in the crystal, *all* vibrational modes become Raman active in the amorphous form (i.e., democracy replaces elitism).[11] The continuum Raman spectrum of *a*-GaAs spans the full range of phonon frequencies which exist in *c*-GaAs. It is noteworthy that the strong low-frequency band in *a*-GaAs, centered at about 70 cm^{-1}, actually corresponds to acoustical phonons in the crystalline form.

As the amorphous bands grow to dominate the spectrum with increasing Si^+ fluence, the crystal LO line weakens, asymmetrically broadens, and shifts downward in frequency. The downshift and asymmetric broadening agree with similar observations reported for As^+-implanted GaAs by Tiong *et al.*[3] This behavior indicates that the crystalline portion of the damage layer is becoming microcrystalline, so that the implanted region becomes an amorphous matrix containing microcrystals surviving from the original bulk crystals. This contradicts an earlier assertion[2] that Si-implanted GaAs remains primarily crystalline at high doses. At the higher fluences, our observed LO-line downshift and broadening imply (via the analysis of Tiong *et al.*[3]) a microcrystallite size of order 40 Å.

Figure 1 reveals that, at high fluence, the structural change saturates and a small crystalline fraction persists within the damage layer. This is a self-annealing phenomenon associated with long implants.[12,13] Fluence was varried by varying implant time, while the ion flux was kept constant for a given ion species. Implant times for the Si implants varied from 7 s (for a fluence of 6×10^{12} cm^{-2}) to 187 min (for a fluence of 1×10^{16} cm^{-2}).

We also report here the first Raman spectra of silicon-implanted GaAs obtained using the SiF_3^+ ion species. This species has a much larger flux, so that the implant time for a given fluence is greatly reduced. (A 10^{16} cm^{-2} SiF_3^+ implant is achieved in 24 min.) Figure 2 compares the effects of implantation with SiF_3^+ and with Si^+, for a fluence of 10^{16} ions/cm^2 with ions of energy 120 keV. Figures 2(c) and 2(a) show the spectra of samples implanted with SiF_3^+ and Si^+, respectively, while Figs. 2(d) and 2(b) show the corresponding spectra observed after the samples were annealed (12-s RTA).

The first-order overall conclusion evident from Fig. 2 is the qualitative *similarity* of the results obtained with SiF_3^+ to those obtained with Si^+. Both implanted samples exhibit the broad bands of amorphous GaAs coexisting with the LO line of a microcrystalline component. After annealing, the amorphous bands essentially disappear, the LO line sharpens, and a sharp TO line appears. All four spectra also reveal weak features near 400 cm^{-1} (shown expanded in Figs. 3 and 4) which, as described in the following section, correspond to silicon local modes. No evidence of fluorine local modes was found in the SiF_3-implanted samples.

Both Figs. 2(a) and 2(c) show that self-annealing is evident in our samples at a fluence of 10^{16} cm^{-2}. Comparing Fig. 2(a) to the set of curves of Fig. 1 yields a closest match to a spectrum intermediate between those of Figs. 1(b) and 1(c), indicating that this has reduced the degree of amorphicity to a level roughy equivalent to that produced by a Si^+ fluence of 10^{13} cm^{-2}. Similarly, for the SiF_3^+ implant of Fig. 2(c), the comparison to Fig. 1 suggests a rough correspondence to a damage level equivalent to that produced by a Si^+ fluence of 10^{14} cm^{-2}.

The previous paragraph, as well as a direct comparison of the two upper curves of Fig. 2, shows that for the same fluence and ion energy, bombardment with SiF_3^+ produces more structural disorder than does Si^+. This is consistent with the greater mass of SiF_3^+. Since SiF_3^+ is heavier than Si^+ (by about a factor of three), the momentum carried by these ions is greater than that carried by equienergetic Si^+ ions (by about a factor of $\sqrt{3}$).

The lower curves of Fig. 2, with the LO dominant and the amorphous bands absent, show that the annealed samples are indeed crystalline and that the damage layer has "healed." However, there is a very interesting difference between these crystal spectra and the original preimplant spectrum of Fig. 1(a): The amplitude of the "forbidden" TO line has increased substantially. This increase is larger for the SiF_3-implanted material, which is recovering from greater damage than is the Si-implanted material.

We interpret the increase in intensity of the TO line as evidence of *departure* from "epitaxial regrowth"; the annealing-induced recrystallization does *not* completely maintain the original (100) orientation, so that the TO line is no longer forbidden. Other possible explanations (for example, phonon-plasmon coupling involving charge carriers in the *n*-type layer, or electric field effects) typically require altered frequency and/or linewidth; the TO lines in Figs. 2(b) and 2(d) have the same position and width as does the TO line in Fig. 1(a). Thus, our results indicate that the implant-and-

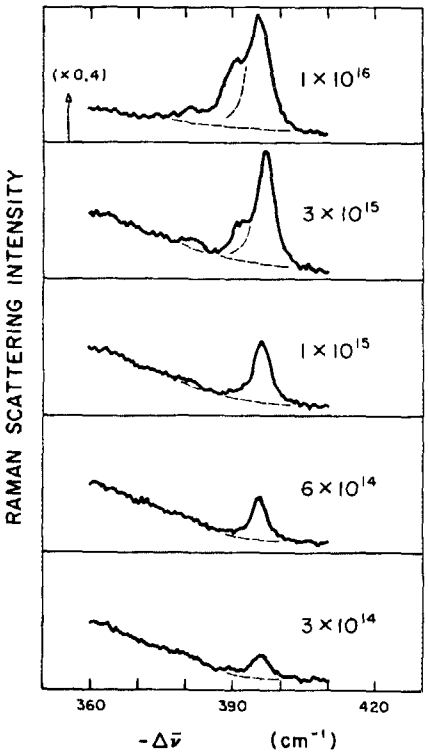

FIG. 4. The effect of fluence on the local-mode Raman spectra of silicon-implanted GaAs. Fluence (of $^{28}Si^+$ ions at 120 keV), in units of ions/cm^2, labels each curve. These samples were given a standard furnace anneal (850 °C, 20 min). Each curve corresponds to about 25 h of data accumulation. The peak of the strongest line, at a fluence of 3×10^{15} cm^{-2}, is about 20 counts/s. The sloping background in these spectra (as well as in the spectra of Fig. 3) is real; it is part of the two-phonon continuum of the host solid.

anneal cycle restores crystallinity but only *incompletely* recovers the initial crystal orientation.

IV. SILICON LOCAL MODES IN IMPLANTED GaAs: THE INFLUENCE OF FLUENCE AND ANNEALING

Figure 3 shows detailed scans of the weak structures seen near 400 cm^{-1} in Fig. 2. Three peaks are observed: at 396, 391, and 381 cm^{-1}. All three are seen after annealing; prior to annealing, only the 396 and 381 cm^{-1} lines are discernible. These spectra are considerably better defined than those seen in recent work by Nakamura and Katoda,[14] and our results provide the first Raman observation of the 381 cm^{-1} line in Si-implanted GaAs. This line is quite important because, unlike the others (as discussed below), it is a Raman signature of Si substituting for Ga in GaAs, i.e., a donor site.

Infrared studies of the vibrational local modes introduced by ^{28}Si in GaAs have recently been carefully analyzed by Theis and Spitzer.[15] Their analysis suggests that our lines at 396, 391, and 381 cm^{-1} correspond to localized vibrations of Si_{As}, Si_{Ga}-Si_{As}, and Si_{Ga} defects, respectively.[16] Si_{Ga} denotes a silicon atom at a gallium site, Si_{As} denotes a silicon atom at an arsenic site, and Si_{Ga}-Si_{As} denotes a nearest-neighbor *pair* of substitutional silicons.

Since annealing results in electrical activation of the implanted region, i.e., its conversion into a low-resistivity *n*-type region, it might be expected that any spectral signature associated with the Si_{Ga} donor would increase after annealing. Thus the fact that the 391 cm^{-1} line is observed after, but not before, annealing would appear to associate this line with Si_{Ga}, rather than with the Si_{Ga}-Si_{As} pair assignment of Theis and Spitzer.

To resolve the apparent contradiction suggested above, and also to test the fluence dependence of these lines, scans were taken for implanted-and-annealed samples for $^{28}Si^+$ fluences F between 10^{16} and 10^{14} cm^{-2}. Results are shown in Fig. 4. The intensity of the 396-cm^{-1} line, which could be followed throughout this range of F, exhibits a systematic sublinear increase with increasing fluence which is approximated well by $I(396)\sim F^{0.7}$. The weak 381 cm^{-1} line, observable above noise only at high F, appears to behave similarly. However, the behavior of the 391 cm^{-1} line is quite different; its intensity increases *much more rapidly* with fluence. The superlinear increase corresponds roughly to $I(391)\sim F^{1.3}$. This means that the relationship between the intensities of the lines at 391 and 396 cm^{-1} is, within experimental error, consistent with $I(391)\sim[I(396)]^2$. Precisely such a relationship is expected if $I(391)$ is produced by a defect composed of a *pair* of impurity atoms. Thus our results *support* the Theis–Spitzer identification of the 391 cm^{-1} line as a local mode of Si_{Ga}-Si_{As}. The explanation of the "appearance" of the 391-cm^{-1} line in the postannealing spectra of Fig. 3 lies elsewhere. Annealing causes all of the local-mode lines to *sharpen* significantly. This sharpening exposes the 391 cm^{-1} line by uncovering it from the low-frequency wing of the stronger line at 396 cm^{-1}. Before annealing, the weaker line is not resolvable.

Throughout this study, we observed no marked differences between the two annealing methods used, SFA and RTA. One illustration of this is the close similarity between the lower-left curve of Fig. 3 (observed for an RTA-annealed sample) and the top curve of Fig. 4 (observed for the corresponding SFA-annealed sample).

Our electrical sheet-resistance measurements showed a clear division of the samples into two electrically disparate groups. All of the implanted-and-annealed samples (such as those whose Raman spectra are shown in Fig. 4 or the lower half of Fig. 3) are *n* type and have sheet resistances in the range of 50–250 Ω/■. All of the unannealed implanted samples (such as those whose spectra are shown in Fig. 1 or the upper half of Fig. 3) have much higher resistance, at least as great as 2×10^4 Ω/■, our measurement limit. Thus the dichotomy in electrical behavior, which corresponds to the execution (or emission) of the SFA or RTA annealing step, is quite evident.

The two benefits of annealing, electrical *activation* and structural *healing*, are widely regarded as two *separate* phenomena. Our experiments strongly suggest that this is *not* the case. Figure 3 reveals *no* annealing-induced increase in the intensity of the Si_{Ga} donor line at 381 cm^{-1}. It therefore appears that the donors are *already* present in the implanted material, and that the high preannealing resistivity is due only to the amorphicity (and consequent low electron moblity) of the damage layer. Annealing then is *not* needed to move and chemically bond Si atoms into Ga sites (they are already there), but is needed simply to allow the *carriers* to

move by recovering the high mobility of the crystalline form.

Electrical conductivity, of course, depends on both carrier concentration and carrier mobility. Our results indicate that the *mobility* factor plays the dominant role in the annealing-induced conductivity increase. This is based on three observations: (1) donor-site silicons are already present before annealing; (2) the first-order effect of annealing is the amorphous-to-crystalline conversion of the host GaAs lattice; (3) the mobility in the amorphous semiconductor (in which transport occurs via tunneling through mid-gap states[11]) is orders of magnitudes smaller than in the crystal. While it may be that an additional effect of the anneal is to increase carrier concentration by decreasing the density of compensating deep traps, the strong mobility effect is *definitely* present via the clear spectroscopic evidence that annealing transforms the amorphous implanted layer into the crystalline semiconductor. Thus, we propose that the mobility increase is the main effect.

It should also be noted that there is a clear precedent for the validity of the notion of substitutionally incorporated donor (and acceptor) impurities in tetrahedrally coordinated amorphous semiconductors. Indeed, the technological importance of hydrogenated amorphous silicon is based on the fact that this material can be doped by the substitutional incorporation, during vapor-phase deposition of the film, of the donor or acceptor impurity atoms.[11,17,18] A significant fraction of the co-deposited impurity atoms enter the covalent network in substitutional sites to render the amorphous semiconductor *n* type or *p* type. These observations lend plausibility to the proposal, made here on the evidence of our Raman experiments, that ion-implanted amorphized semiconductors contain a large concentration of substitutionally sited implant atoms *prior* to the annealing step.

The annealing-induced sharpening of the local-mode lines, evident in a comparison of the upper and lower spectra of Fig. 3, can be understood as a narrowing of the distribution of local environments sampled by the four-coordinated silicons. In the amorphous material, there is a spread in nearest-neighbor bond angles in excess of the (dynamic) bond-angle spread of the crystal.[11] This static-disorder contribution to the bond-angle dispersion disappears upon annealing (recrystallization).

V. SUMMARY

Raman-scattering experiments were carried out on a variety of implanted and implanted-and-annealed GaAs samples, using both Si^+ and SiF_3^+ as the implant species, in order to probe the influence of processing on the atomic-scale structure of the implanted region. For given fluence and ion energy, SiF_3^+ ions are more effective than Si^+ ions in damaging the lattice; otherwise, effects observed with the two types of ions are qualitatively quite similar. The progressive amorphization, with increasing fluence, of a 1000-Å-deep portion of the damage layer, was clearly observed (Fig. 1) via the evolution of the broad three-band continuum characteristic of amorphous GaAs. The continuum was measured from its high-frequency cutoff near 300 cm^{-1} down to about 15 cm^{-1}. The crystalline remnant at high fluence is microcrystalline, as revealed by the broadening and downshifting of the crystal LO line. Annealing fully recovers the crystalline form, but the (100) orientation does *not* fully recover, as revealed (Fig. 2) by the appreciable increase of the TO line. This calls into question the widely made assumption of epitaxial regrowth.

Three lines observed near 400 cm^{-1} in heavily implanted samples (Fig. 3) were identified with silicon local modes by comparison with recent infrared work and by measurements of their fluence dependence (Fig. 4). In particular, our fluence-dependence results support a previous assignment of the 391 cm^{-1} line to a defect made up of a neighboring *pair* of silicon impurities. We also report the first Raman-scattering observation of a line associated with the Si_{Ga} donor site (381 cm^{-1}). The effect of annealing on the silicon-local-mode lines, displayed in Fig. 3, is *not* found to be an intensity increase, but instead is seen to be pronounced line *narrowing* which we interpret as reflecting an annealing-induced sharpening of the distribution of local environments encountered by the substitutional silicons. In particular, the Si_{Ga} donor-site line is clearly seen *before* annealing, even though annealing is necessary to transform the highly resistive implanted material into semiconducting *n*-type GaAs. These results strongly suggest that the primary role of annealing in the "electrical activation" of implanted semiconductors is *not* to shift the impurity atoms into substitutional donor or acceptor sites (they already occupy such sites), but is instead to recover the high carrier mobility of the crystalline form. In the low-mobility amorphous material which forms the host solid after implantation and before annealing, the carriers are present, but immobile. "Healing" and "activation" thus correspond to the *same* structural process, the elimination of amorphicity.

ACKNOWLEDGMENTS

The authors gratefully acknowledge the technical expertise of S. W. Bond, and thank him for performing the ion implantations. We are also indebted to Guofu Feng for UV reflectivity measurements confirming the high crystal quality of the preimplant material. This work was supported in part by the Institute of Materials Science and Engineering of the Virginia Center for Innovative Technology.

[1] D. E. Aspnes, S. M. Kelso, C. G. Olson, and D. W. Lynch, Phys. Rev. Lett. **48**, 1863 (1982).
[2] T. Nakamura and T. Katoda, J. Appl. Phys. **53**, 5870 (1982).
[3] K. K. Tiong, P. M. Amirtharaj, F. H. Pollak, and D. E. Aspnes, Appl. Phys. Lett. **44**, 122 (1984).
[4] F. H. Pollak and R. Tsu, in *Proceedings of the Society of Photo-optical Instrumentation Engineers, Vol. 452, Spectroscopic Techniques for Semiconductor Technology* (SPIE, Bellingham, 1984), p. 26; F. H. Pollak, SRI Report on Microelectronics Materials (1985) (unpublished).
[5] D. E. Aspnes and A. A. Studna, Phys. Rev. B **27**, 985 (1983).
[6] M-L. Theye and A. Gheorghiu, Sol. Energy Mater. **8**, 331 (1982).
[7] R. G. Wilson and V. R. Deline, Appl. Phys. Lett. **37**, 793 (1980).
[8] W. Hayes and R. Loudon, *Scattering of Light by Crystals* (Wiley, New York, 1978).
[9] M. Wihl, M. Cardona, and J. Tauc, J. Non-Cryst. Solids **8-10**, 172 (1972).
[10] L. L. Abels, S. Sundaram, R. L. Schmidt, and J. Comas, Appl. Surf. Sci. **9**, 2 (1981).
[11] R. Zallen, *The Physics of Amorphous Solids* (Wiley, New York, 1983).
[12] R. S. Bhattacharya, A. K. Rai, Y. K. Yeo, P. P. Pronko, S. C. Ling, S. R.

Wilson, and Y. S. Park, J. Appl. Phys. **54**, 2329 (1983).
[13]Self-annealing, usually attributed to a temperature rise, is a poorly understood phenomenon currently under study in several laboratories, including ours.
[14]T. Nakamura and T. Katoda, J. Appl. Phys. **57**, 1084 (1985).
[15]W. M. Theis and W. G. Spitzer, J. Appl. Phys. **56**, 890 (1984).
[16]Our peak positions are about 2.5 cm^{-1} lower in $\bar{\nu}$ than the corresponding infrared peaks listed by Theis and Spitzer in their Table II. This represents the temperature-induced red shift: Our experiments were done at 300 K, Theis and Spitzer's at 80 K.
[17]W. E. Spear and P. G. LeComber, Solid State Commun. **17**, 1193 (1975); Philos. Mag. **33**, 935 (1976).
[18]W. Paul, A. J. Lewis Jr., G. A. N. Connell, and T. D. Moustakis, Solid State Commun. **20**, 969 (1976).